



## Search for standard model Higgs boson with trileptons and missing transverse energy with $9.7 \text{ fb}^{-1}$ of $p\bar{p}$ collisions at $\sqrt{s} = 1.96 \text{ TeV}$

The DØ Collaboration  
URL <http://www-d0.fnal.gov>  
(Dated: February 28, 2012)

A search for the standard model (SM) Higgs boson is presented using a trilepton sample, using electrons and muons in the  $ee\mu$  and  $\mu\mu e$  final states, produced in  $p\bar{p}$  collisions at  $\sqrt{s} = 1.96 \text{ TeV}$ . Data collected from April 2002 to September 2011 by the RunII DØ detector corresponds to  $9.7 \text{ fb}^{-1}$  of integrated luminosity. No excess is observed above the SM background and limits are extracted on the SM Higgs boson production cross section for a Higgs mass range of  $m_H = 100 - 200 \text{ GeV}$ , in intervals of 5 GeV.

*Preliminary Results for Winter 2012 Conferences*

## I. INTRODUCTION

At the Tevatron, associated production of  $q\bar{q} \rightarrow WH$  and  $q\bar{q} \rightarrow ZH$  have some of the highest cross section production rates for final states containing a SM Higgs boson, second only to gluon-gluon fusion Higgs production. Furthermore, since the  $H \rightarrow WW$  decay modes dominate the branching ratios of the Higgs boson in the standard model (SM) for Higgs boson masses above  $m_H = 135$  GeV, this makes  $VH \rightarrow VWW$  (where  $V$  is either a  $W$  or a  $Z$  boson) a good process to use to search for the Higgs boson. The hadronic decays of the  $W$  bosons have high branching fractions, but suffers from a large hadronic background that is difficult to separate from the signal. Despite having a low 9.4%(3.4%) branching fraction, the leptonic decays of the  $W(Z)$  bosons provide a more sensitive final state search at the Tevatron. The  $H \rightarrow WW \rightarrow \ell\nu\ell\nu$  decay suffers from a large  $Z \rightarrow \ell\ell$  background. By requiring a third lepton, this background becomes more manageable. Contributions from gluon fusion Higgs production decaying via  $H \rightarrow ZZ$  are significant in the trilepton final states and are included in the signal modeling, along with the less significant  $gg \rightarrow H \rightarrow WW$  process and vector boson fusion  $VV \rightarrow H$  production.

We present a search for the Higgs boson with a final state containing at least three isolated leptons, either electrons or muons, and missing transverse momentum – defined as the energy imbalance in the transverse plane ( $\cancel{E}_T$ ). Due to the better sensitivity and lower backgrounds, we focus on the  $ee\mu$  and  $\mu\mu e$  final states. This analysis was performed on the Run II dataset recorded between April 2002 and September 2011, corresponding to  $9.7 \text{ fb}^{-1}$  of integrated luminosity.

## II. DØ DETECTOR

In order to identify electrons, muons, and missing transverse momentum, we use the multi-purpose DØ detector. The central-tracking system consists of a silicon microstrip tracker (SMT) and a central fiber tracker (CFT), both contained within a 2 T superconducting solenoidal magnet [1]. The SMT has  $\approx 800,000$  individual strips, with typical pitch of  $50-80 \mu\text{m}$ , and a design optimized for tracking and vertexing capability at pseudorapidities of  $|\eta| < 2.5$ . Here we define  $\eta = -\ln(\tan \theta/2)$ , where  $\theta$  is the polar angle relative to the proton beam direction. The SMT has a six-barrel longitudinal structure, each with a set of four layers arranged axially around the beam pipe, and interspersed with 16 radial disks. A new layer of silicon (Layer 0) was added just outside the beam pipe in 2006 to help with vertexing [2]. The CFT has eight concentric coaxial barrels, each consisting of two doublet layers of overlapping scintillating fibers. The inner-most double layer is parallel to the collision axis, while the second alternates by  $\pm 3^\circ$  relative to the axis.

Central and forward preshower detectors are located just outside of the solenoid, but before the calorimetry, to help measure the energy loss associated with particles traveling through the solenoid material. The calorimetry system consists of three liquid-argon sampling calorimeters: a central section (CC) covering  $|\eta|$  up to  $\approx 1.1$ , and two end calorimeters (EC) that extend coverage to  $|\eta| \approx 4.2$ , housed in separate cryostats [3]. In an attempt to include the intercryostat region (ICR) where there is incomplete calorimeter coverage, scintillators between the CC and EC provide sampling of developing showers at  $1.1 < |\eta| < 1.4$ .

A muon system [4] resides beyond the calorimeters, and consists of a layer of tracking detectors and scintillation trigger counters before 1.8 T toroids, followed by two similar layers after the toroids. Tracking at  $|\eta| < 1$  relies on 10 cm wide drift tubes [3], while 1 cm mini-drift tubes are used at  $1 < |\eta| < 2$ .

Luminosity is measured with two arrays of 24 plastic scintillator counters each, located in front of the EC cryostats ( $2.7 < |\eta| < 4.4$ ), using a method that relies on counting the number of beam crossings with zero interactions. Trigger and data acquisition systems are designed to accommodate the high luminosities of Run II. Based on preliminary information from all three sub-systems, the output of the first level of triggering is used to limit the rate for accepted events to  $\approx 1.5$  kHz. At the next trigger stage, with more refined information, the rate is reduced further to  $\approx 0.8$  kHz. These first two levels of triggering rely mainly on hardware and firmware. The third and final level of the trigger, with access to all the event information, uses software algorithms and a computing farm to make decisions, and further reduces the output rate to  $\approx 100$  Hz, which is then written to tape.

## III. DATA AND MONTE CARLO SAMPLES

The data sample used in this analysis was collected between April 2002 and September 2011 (Run II), and corresponds to an integrated luminosity of  $9.7 \text{ fb}^{-1}$  for the trilepton final state after imposing data quality requirements. To maximize our signal acceptance, we use all events collected by DØ that pass our event selection without requiring a specific trigger to fire.

The signal and  $WW$ ,  $WZ$ , and  $ZZ$  diboson SM backgrounds have been generated using PYTHIA [5]. The  $Z/\gamma^* + \text{jet}$  and  $t\bar{t}$  backgrounds are modeled using ALPGEN [6], with PYTHIA used to model the jet hadronization. All of the

MC is passed through a GEANT [7] simulation of the DØ detector.

For the  $\mu\mu e$  final state, we model the  $Z + \gamma$  background using a data driven method, where reconstructed  $\mu\mu\gamma$  events are reweighed by a  $\gamma \rightarrow e$  fake ratio to match the  $Z + \gamma$  background in data. To estimate the  $\gamma \rightarrow e$  fake ratio, we consider events with 2 identified muons and a photon (see below) with  $\cancel{E}_T < 20$  GeV and a  $\mu\mu\gamma$  invariant mass between 75 and 105 GeV. This kinematic region is dominated by  $Z \rightarrow \mu\mu$  decays with final state photon radiation, and we take the ratio of the number of events reconstructed as photons to that reconstructed as electrons as our fake ratio. We then apply this fake ratio to data  $\mu\mu\gamma$  events outside this region to estimate the  $\mu\mu\gamma \rightarrow \mu\mu e$  background.

#### IV. EVENT SELECTION

To increase signal acceptance, all events satisfying any trigger of the DØ trigger suite are accepted for this analysis. While most events selected in the analysis are triggered by single-lepton and dilepton triggers, additional acceptance is gained by including triggers with jets or missing transverse energy. The simulated background samples are normalized to the integrated luminosity and appropriate cross sections.

Electrons are reconstructed using information from the calorimetry and tracking systems. Electromagnetic (EM) showers are identified in the calorimeter by comparing the longitudinal and transverse shower profiles to those of simulated electrons. The fraction of energy deposited in the EM layers, compared to the total energy deposited in the calorimetry system, must be greater than 90%. A shower must be isolated, as measured from the calorimeter energy information, have a transverse momentum ( $p_T$ ) greater than 10 GeV, and be within the acceptance of the calorimeter ( $|\eta| < 1.1$  in the CC or  $1.5 < |\eta| < 2.5$  in the EC). Neutral Network outputs and an electron likelihood are used to further separate electrons from hadronic showers. To help reduce the photon background contribution, the shower must be matched to a track found in the central tracker. In the CC region, it is also required that the ratio of the cluster's energy to the track's transverse momentum ( $E_T^{\text{cluster}}/p_T^{\text{track}}$ ) be less than eight. Due to less well-known energy resolutions, electrons reconstructed in the ICR are not considered. All other electrons, found either in the fiducial or non-fiducial regions, are kept.

Photons reconstructed in data are used to model the  $Z + \gamma$  background in the  $\mu\mu e$  final state. Like electrons, photons are reconstructed using information from the calorimetry and tracking systems. The EM shower is reconstructed in the calorimeter with an EM fraction greater than 95%, with similar calorimeter isolation and detector  $\eta$  cuts as those used to reconstruct electrons. A Neutral Network is also used to distinguish photons from jets. The most significant difference between the electron and photon reconstruction is in the tracker; we require that there be no track pointing to the photon. In addition, we require that there be little activity in the tracker along the paths that an electron with a  $p_T$  consistent with the photon's  $p_T$  would have traveled.

Muon tracks are reconstructed from hits in the wire chambers and scintillators in the muon system. The muon tracks then must be matched to tracks in the central tracker with transverse momentum greater than 10 GeV. Muon reconstruction is restricted to the coverage of the muon system,  $|\eta| < 2.0$ . The distance of closest approach of the muon track to the beamline,  $dca$ , satisfy the requirement  $|dca| < 0.04(0.2)$  cm for tracks with(no) SMT hits. The track must also have a reconstruction  $\chi^2$  per degrees of freedom less than 9.5 and at least two CFT hits. To identify isolated muons, the scalar sum of the transverse momenta of all the tracks inside a  $\Delta\mathcal{R} < 0.5$  cone around the muon track with the exception of the muon track itself must be less than  $0.2 \times p_T^\mu$ . Here we defined  $\Delta\mathcal{R} = \sqrt{(\Delta\phi)^2 + (\Delta\eta)^2}$ , where  $\phi$  is the azimuthal angle. Similarly, the scalar sum of the transverse energies of all calorimeter clusters inside a hollow cone  $0.1 < \Delta\mathcal{R} < 0.4$  around the muon must be less than  $0.2 \times p_T^\mu$ . These scaled isolation requirements are used to help reject low- $p_T$  muons from heavy flavor decays and maximize the efficiency of high- $p_T$  prompt muons. Cosmic ray muons are suppressed by requiring a timing criterion on the hits in the scintillator layers.

The missing transverse energy,  $\cancel{E}_T$ , is obtained from a vector sum of the transverse components of calorimeter energy depositions and corrected for identified muons. Modified MET variables,  $\cancel{E}_T^{\text{special}}$  and  $\cancel{E}_T^{\text{significance}}$ , are used to discriminate events with real  $\cancel{E}_T$  from events where the  $\cancel{E}_T$  arises from mismeasurement. The  $\cancel{E}_T^{\text{special}}$  variable assigns less significance to the missing energy in an event when the opening angle,  $\Delta\phi$ , between the  $\cancel{E}_T$  and any other lepton or jet is small, as this may be a potential source of mismeasurement. The  $\cancel{E}_T^{\text{special}}$  is defined as follows:  $\cancel{E}_T$  if  $\Delta\phi(\cancel{E}_T, \text{nearest lepton/jet}) > \pi/2$  or  $\cancel{E}_T \times \sin(\Delta\phi(\cancel{E}_T, \text{nearest lepton/jet}))$  otherwise. A  $\cancel{E}_T^{\text{significance}}$  is the difference, expressed in standard deviations, between the measured  $\cancel{E}_T$  and 0.

We select events with three isolated, highly-energetic leptons (two of the same flavor -  $\ell_1, \ell_2$ , while the third is not -  $\ell'_3$ ) that originate from the same position (within 3 cm) along the beamline. In both channels the transverse momenta must satisfy  $p_T^{\ell_1} > 15$  GeV,  $p_T^{\ell_2} > 10$  GeV, and  $p_T^{\ell'_3} > 10$  GeV. In addition, the same flavor dilepton invariant mass is required to be greater than 15 GeV. To ensure that the leptons originate from  $p\bar{p}$  collision, we require that their position along the beamline at the distance of closest approach to the interaction point,  $z_{dca}$ , be less than 3 cm from the other 2 leptons. An additional cut is made in the  $ee\mu$  channel where the minimal  $z_{dca}$  distance between the

Samples	$ee\mu$ final	$\mu\mu e$ final
Data	96	69
Signal	1.39	0.78
$WH$	0.55	0.41
$ZH$	0.57	0.33
$HZZ$	0.26	0.03
$HWW$	0.01	< 0.01
$VBF$	< 0.01	< 0.01
Total Background	$89.20 \pm 2.36$	$60.34 \pm 2.44$
$Z \rightarrow ee + jets$	$48.26 \pm 2.23$	–
$Z \rightarrow \mu\mu + jets$	–	$9.81 \pm 0.82$
$Z \rightarrow \tau\tau + jets$	$4.33 \pm 0.64$	$0.26 \pm 0.12$
$Z\gamma$	–	$27.62 \pm 1.46$
$WZ$	$23.45 \pm 0.35$	$19.40 \pm 0.21$
$ZZ$	$11.09 \pm 0.16$	$2.35 \pm 0.07$
$WW$	$0.69 \pm 0.13$	$0.15 \pm 0.05$
$t\bar{t}$	$1.38 \pm 0.07$	$0.74 \pm 0.05$

TABLE I: Expected yields for  $m_H = 145$  GeV for the complete RunII dataset. Uncertainties shown are based only on the statistical uncertainties on the number of generated background events.

muon and either of the two electrons must be less than 1 cm. This is to help remove muons produced by either other collisions in the event or cosmic rays.

We exclude  $\mu\mu e$  events with  $\cancel{E}_T$  less than 20 GeV that have a  $\mu\mu e$  invariant mass between 75 and 105 GeV, as these events were used to assess the  $Z\gamma$  fake rate. As a further cleanup cut, we require that the  $\cancel{E}_T^{special}$  be greater than 15 GeV or that that the  $\cancel{E}_T^{significance}$  be greater than 3.0.

The  $\mu\mu e$  final state requires the additional condition that there be one and only one electron in the event, as to not overlap with the  $ee\mu$  channel.

The transverse mass is defined as  $M_T = \sqrt{2 \cdot p_T^\ell \cdot \cancel{E}_T \cdot (1 - \cos\Delta\phi(\ell, \cancel{E}_T))}$ , with the minimum transverse mass between the two same flavor leptons defined as  $M_T^{min} = \min(M_T(\ell_1, \cancel{E}_T), M_T(\ell_2, \cancel{E}_T))$ .

The final  $ee\mu$  and  $\mu\mu e$  yields for  $m_H = 145$  GeV are shown in Table I for RunII. The  $W + jets$  sample is negligible and has been dropped from the training background sample and the limits setting process.

Figures 1 and 2 shows the 12 distributions used in the  $ee\mu$  multivariate analysis (MVA) method discussed in Sec. V; Figures 3 – 5 show the 16 distributions used in the  $\mu\mu e$  MVA.

## V. FINAL DISCRIMINANTS

At the final selection, the signal is separated from the remaining background using a gradient boosted decision tree (BDT) technique for the  $ee\mu$  channel and a randomised forest (RF) BDT configuration for the  $\mu\mu e$  channel. The final discriminant BDT uses as inputs the following variables:

- $ee\mu$  channel
  - invariant mass of the di-electron pair ( $M_{e_1 e_2}$ );
  - invariant mass of the tripleton system with the  $\cancel{E}_T$ , where the  $\cancel{E}_T$  is assumed to have  $\eta = 0$  ( $M_{e_1 e_2 \mu \cancel{E}_T}$ );
  - minimum transverse mass between the  $\cancel{E}_T$  and either electron ( $M_T^{min}$ );
  - transverse momentum for the trailing electron ( $p_T^{e_2}$ );
  - transverse momentum of the di-electron pair ( $p_T^{e_1 e_2}$ );
  - transverse momentum of the di-electron pair with the muon ( $p_T^{e_1 e_2 \mu}$ );
  - $\cancel{E}_T^{special}$ ;
  - $\cancel{E}_T^{significance}$ ;
  - opening angle in  $\phi$  between the di-electron pair ( $\Delta\phi_{e_1, e_2}$ );
  - opening angle in  $\phi$  between the di-electron system and the muon ( $\Delta\phi_{e_1 e_2, \mu}$ );

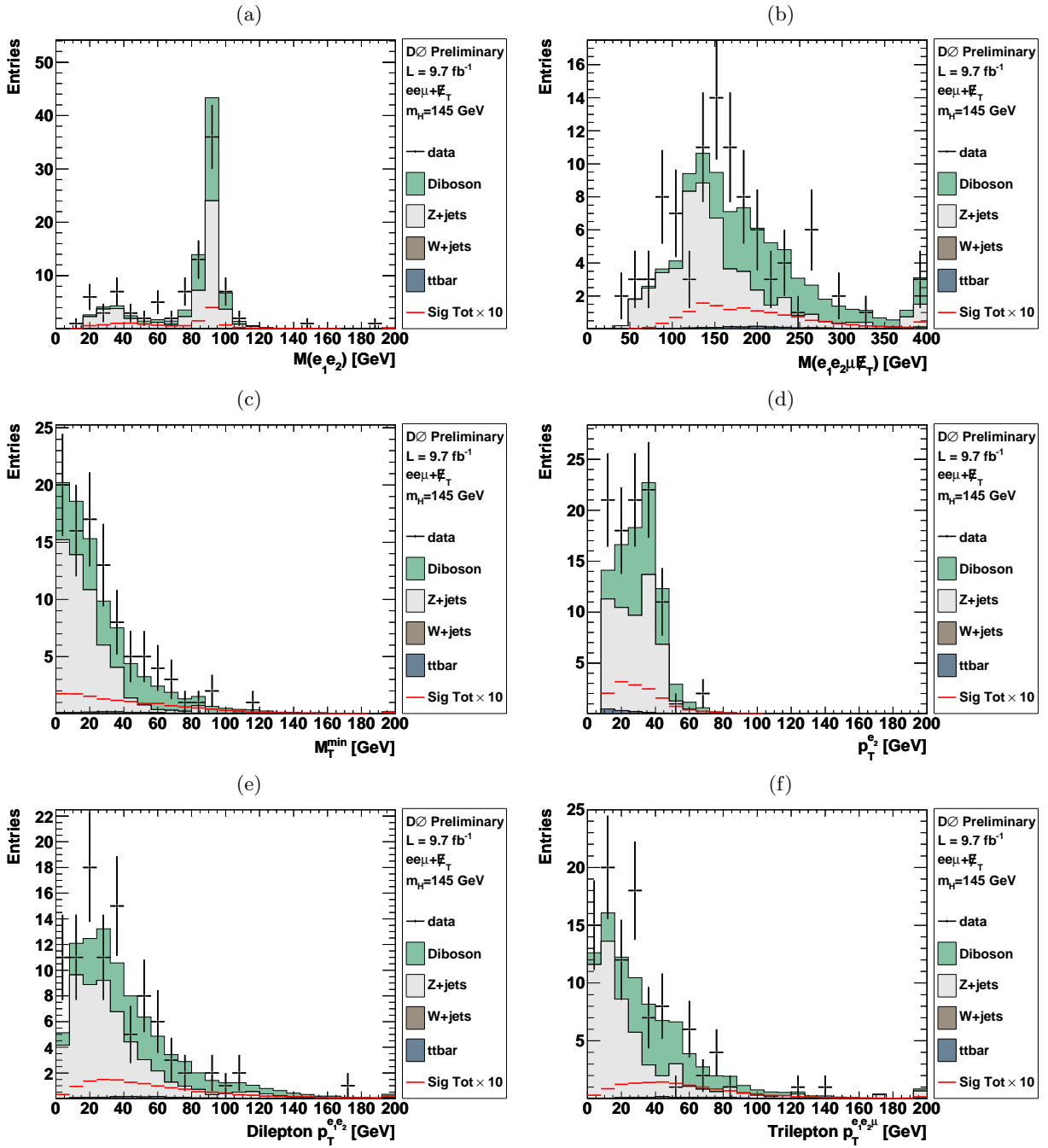


FIG. 1: The (a) di-electron mass, (b) trilepton +  $\cancel{E}_T$  mass, (c) minimum transverse mass between either electron and the  $\cancel{E}_T$ , (d) transverse momentum of the trailing electron, (e) transverse momentum of the di-electron system, and (f) transverse momentum of the trilepton system. The expected signal, multiplied by 10, for a 145 GeV SM Higgs is shown. The highest bin includes all events above the upper range of the histogram (b).

- opening angle in  $\eta$  and  $\phi$  space between the closest two leptons ( $\min(\Delta\mathcal{R}_{\ell_i, \ell_j})$ );
- opening angle in  $\eta$  and  $\phi$  space between the second closest two leptons ( $\text{med}(\Delta\mathcal{R}_{\ell_i, \ell_j})$ ).

- $\mu\mu e$  channel

- the di-muon invariant mass ( $M_{\mu_1\mu_2}$ );
- invariant mass of the di-muon pair, electron, and missing transverse energy, where the  $\cancel{E}_T$  is assumed to have an  $\eta = 0$  ( $M_{\mu_1\mu_2 e \cancel{E}_T}$ );

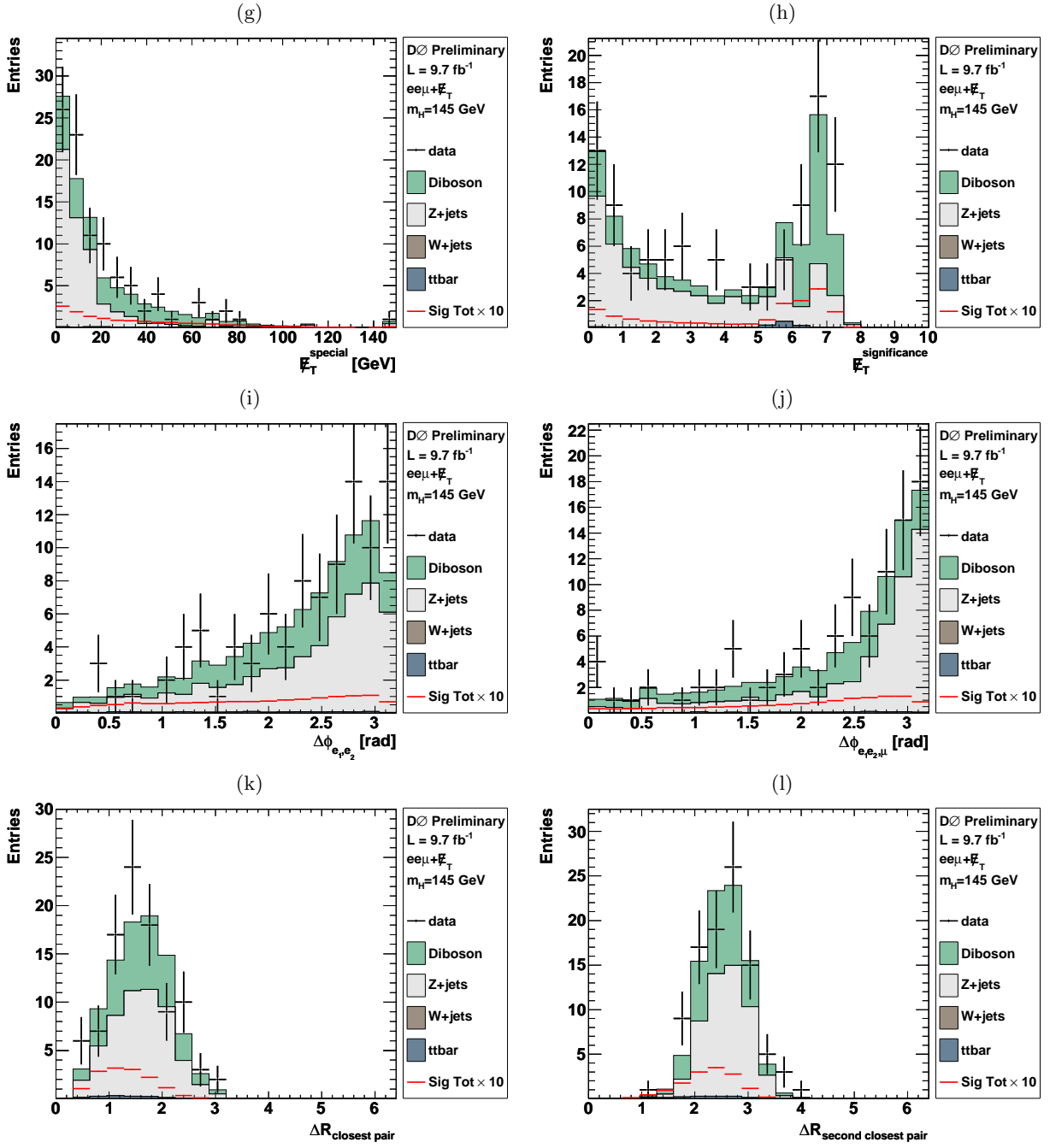


FIG. 2: The (g)  $E_T^{special}$ , (h)  $E_T^{significance}$ , (i)  $\Delta\phi$  between the two electrons, (j)  $\Delta\phi$  between di-electron system and the muon, (k)  $\Delta R$  between the closest two leptons, and (l)  $\Delta R$  between the second closest two leptons. The expected signal, multiplied by 10, for a 145 GeV SM Higgs is shown. The highest bin includes all events above the upper range of the histogram (h).

- minimum of transverse mass between the  $E_T$  and either the leading or trailing muon ( $M_T^{min}$ );
- transverse momentum of the electron ( $p_T^e$ );
- transverse momentum of the di-muon pair with the electron ( $p_T^{\mu_1\mu_2e}$ );
- pseudorapidity of the di-muon pair with the electron ( $\eta_{\mu_1\mu_2e}$ );
- scalar sum of the three leptons' transverse momenta plus the  $E_T$  ( $\sum_i p_T^i + E_T$ );

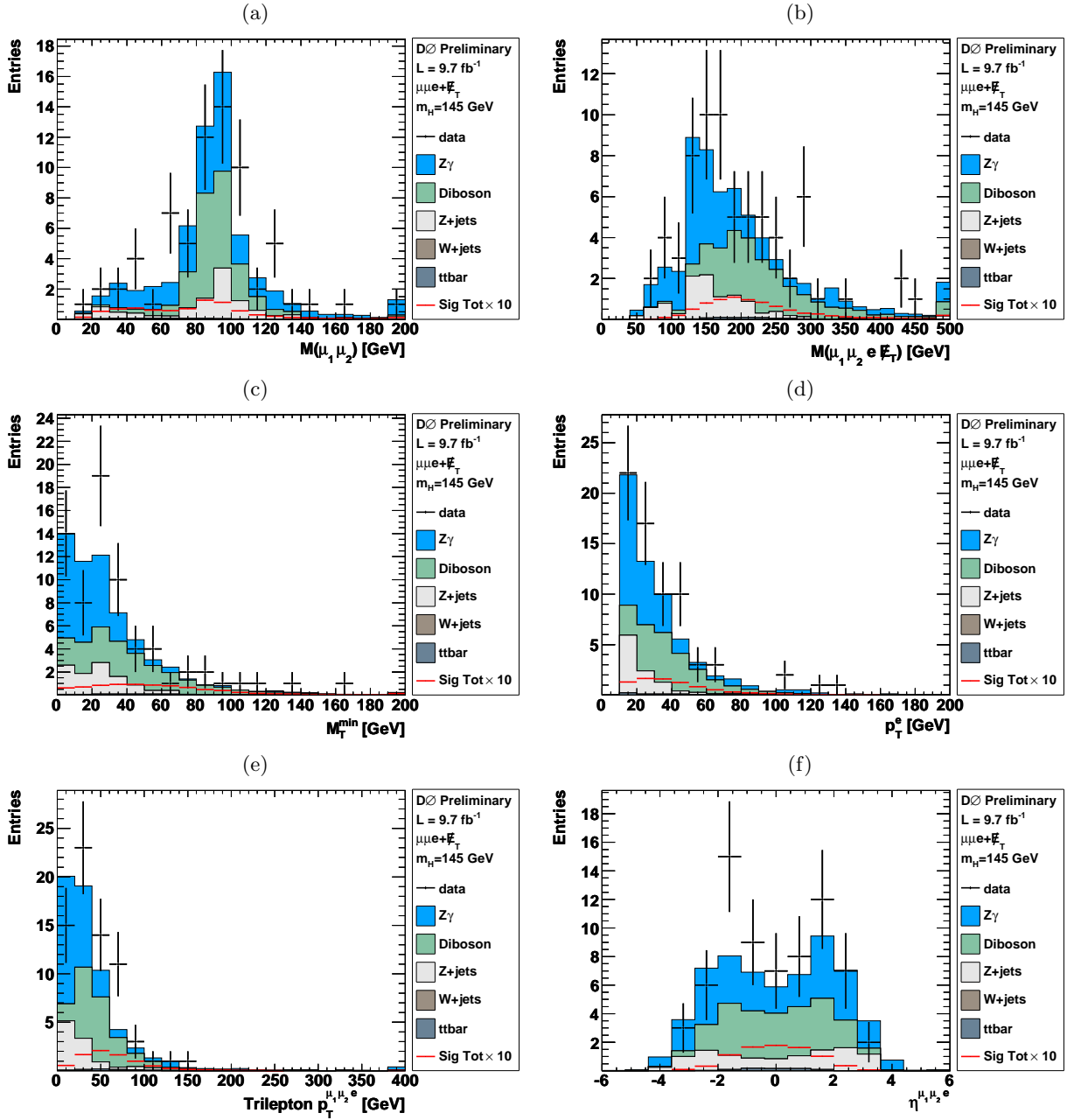


FIG. 3: The (a) di-muon mass, (b) trilepton +  $\cancel{E}_T$  mass, (c) minimum transverse mass between either muon and the  $\cancel{E}_T$ , (d) transverse momentum of the electron, (e) transverse momentum of the di-muon pair with the electron, and (f) physics  $\eta$  of the trilepton system. The expected signal, multiplied by 10, for a 145 GeV SM Higgs is shown. The highest bin includes all events above the upper range of the histogram (a,b,e).

- $\cancel{E}_T$  significance;
- $\cancel{E}_T$  special;
- transverse mass between the  $\cancel{E}_T$  and the electron ( $M_T^{(e, \cancel{E}_T)}$ );
- mt2 medium - the “mt2” variable was proposed in [8], is similar to the transverse mass, but extended to a final state with two visible particles and two invisible ones. We compute the variable as in [9], using an algorithm provided by the authors. Because we have 3 visible particles in our final state, we calculate three mt2 variables, one for each combination. We order the three mt2 values, and use the middle value in the discriminant;

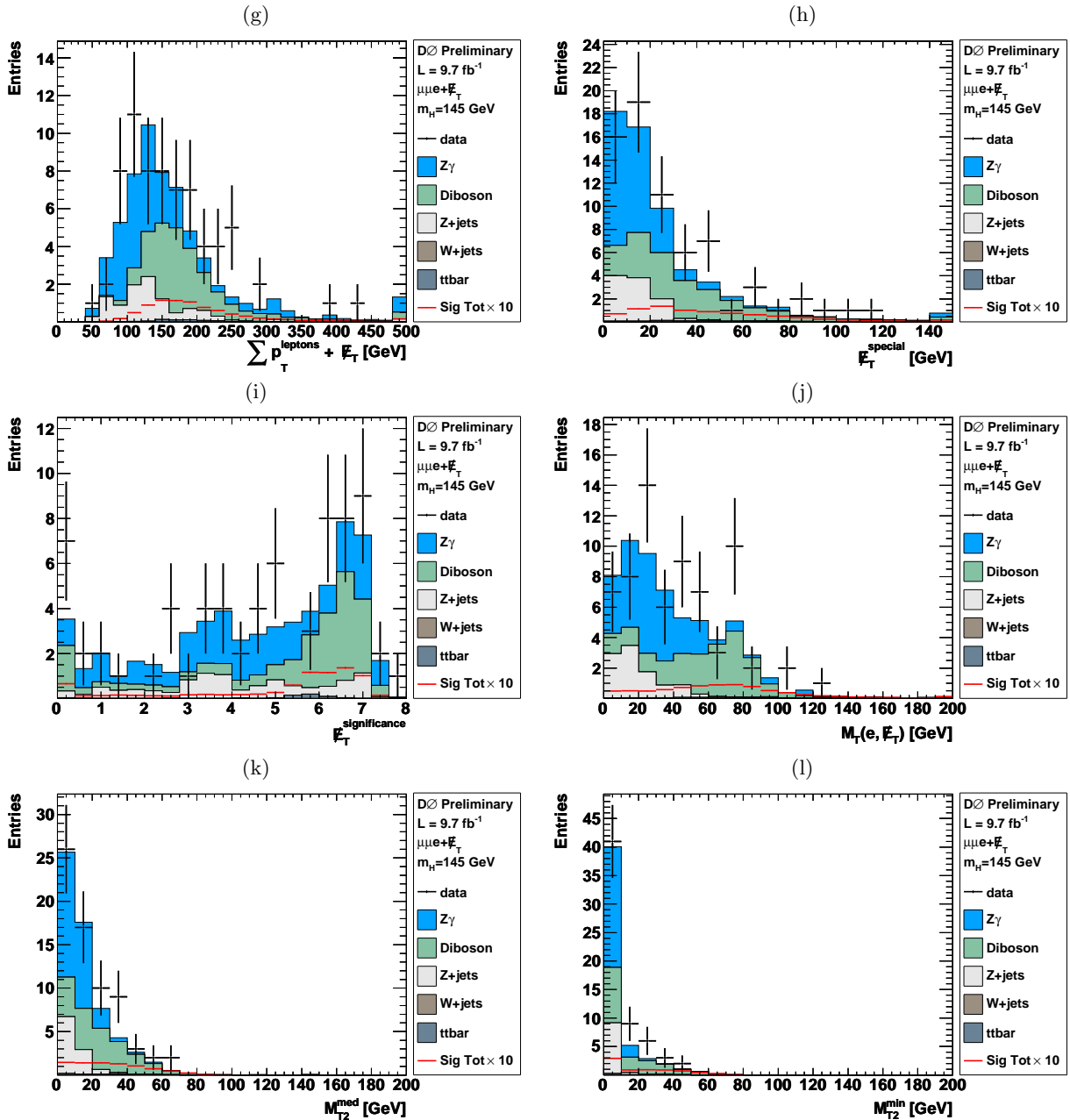


FIG. 4: The (g) scalar sum of the leptons'  $p_{T\text{'s}}$  and  $\cancel{E}_T$ , (h)  $\cancel{E}_T^{\text{special}}$ , (i)  $\cancel{E}_T^{\text{significance}}$ , (j) transverse mass between the electron and the  $\cancel{E}_T$ , (k) second lowest  $m_{T2}$  transverse mass, and (l) the minimum  $m_{T2}$  transverse mass. The expected signal, multiplied by 10, for a 145 GeV SM Higgs is shown. The highest bin includes all events above the upper range of the histogram (g,h).

- $m_{T2}$  minimum - smallest  $m_{T2}$  value of the three possible combinations;
- opening angle in  $\eta$  and  $\phi$  space between the closest two leptons ( $\min(\Delta\mathcal{R}_{\ell_i, \ell_j})$ );
- minimum opening angle in  $\phi$  between the  $\cancel{E}_T$  and either the leading or trailing muon ( $\min(\Delta\phi_{\mu_1, \cancel{E}_T}, \Delta\phi_{\mu_2, \cancel{E}_T})$ );
- opening angle in  $\phi$  between the di-muon system and the electron ( $\Delta\phi_{\mu_1\mu_2, e}$ );
- opening angle in  $\phi$  between the two muons.

Simulated events are used to train the BDT to differentiate between  $WH$  and  $ZH$  signal events and all background events (diboson,  $t\bar{t}$ ,  $Z/\gamma^*$ ,  $W$  boson, etc.). The DTs are trained for each of the Higgs mass points from  $m_H = 100 -$

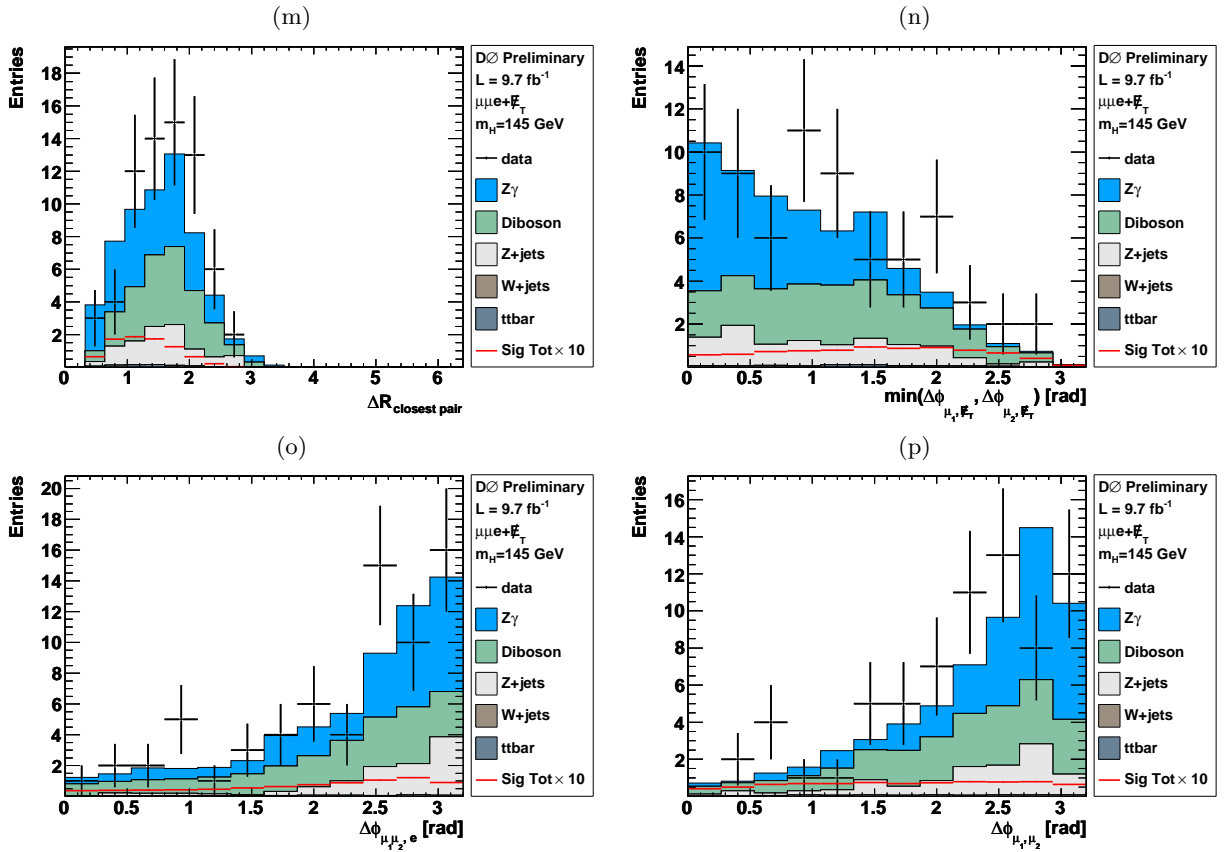


FIG. 5: The (m)  $\Delta\mathcal{R}$  between the closest two leptons, (n) minimum  $\Delta\phi$  between either muon and the  $\cancel{E}_T$ , (o)  $\Delta\phi$  between di-muon system and the electron, and (p)  $\Delta\phi$  between the two muons. The expected signal, multiplied by 10, for a 145 GeV SM Higgs is shown. The highest bin includes all events above the upper range of the histogram.

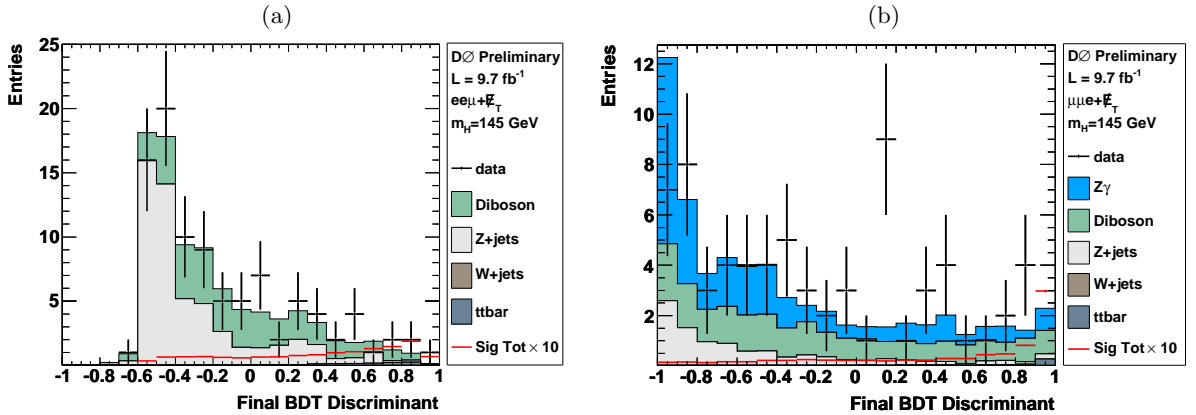


FIG. 6: Final BDT discriminant for (a)  $ee\mu$  channel and (b)  $\mu\mu e$  channel. The discriminant shown is trained for a Higgs mass of 145 GeV, shown multiplied by 10.

200 GeV in intervals of 5 GeV.

TABLE II: Expected and observed upper limits at 95% CL for  $\sigma(p\bar{p} \rightarrow H + X)$  relative to the SM for the total combination and separately for the  $ee\mu$  and  $\mu\mu e$  channels in Run II for different Higgs boson masses ( $m_H$ ).

$m_H$ (GeV/ $c^2$ )	100	105	110	115	120	125	130	135	140	145	150
Exp. all	15.82	16.46	16.54	15.25	13.34	12.25	9.57	8.29	7.99	7.41	7.01
Obs. all	30.78	40.39	30.30	29.68	22.30	18.42	16.75	12.72	10.78	9.69	8.24
Exp. $ee\mu$	19.09	19.84	20.29	18.30	16.03	15.28	12.29	10.81	10.27	9.54	9.16
Obs. $ee\mu$	36.22	40.97	30.83	29.11	24.94	22.24	19.23	16.06	13.82	14.17	11.97
Exp. $\mu\mu e$	30.73	33.18	32.04	27.11	25.55	20.74	16.58	16.08	14.46	12.97	11.84
Obs. $\mu\mu e$	44.41	63.71	54.39	55.16	38.32	30.74	26.48	20.37	17.65	13.80	13.03

$m_H$ (GeV/ $c^2$ )	155	160	165	170	175	180	185	190	195	200
Exp. all	7.14	7.13	7.07	7.74	8.64	9.72	10.74	12.29	13.20	14.67
Obs. all	8.82	7.46	7.24	7.27	9.63	9.65	10.66	13.89	13.30	16.54
Exp. $ee\mu$	9.13	9.70	9.73	10.35	11.98	13.31	13.83	15.45	16.35	17.80
Obs. $ee\mu$	11.79	11.73	11.75	11.46	12.36	13.59	15.29	13.64	13.79	16.69
Exp. $\mu\mu e$	13.01	12.53	12.36	13.75	14.97	16.46	18.74	21.80	25.19	25.87
Obs. $\mu\mu e$	15.00	11.59	10.66	13.20	19.11	19.53	19.41	35.76	36.34	40.64

## VI. SYSTEMATIC UNCERTAINTIES

To account for the lepton ID efficiencies, a 2.5%(4%) systematic is applied for each electron(muon) in the final state. A PDF uncertainty of 2.5% and a trigger efficiency uncertainty of 3.5% is applied to both the signal and background MC samples. We assign a 6.2% theoretical cross section uncertainty to the associated production ( $VH$ ) signals, a 5% cross section uncertainty to the gluon-gluon fusion ( $ggH, H \rightarrow VV$ ) signals, and a 4.9% uncertainty on the vector boson fusion ( $VBF$ ) signal. A 6% theoretical cross section uncertainty is applied to the diboson background MC, while a 7% uncertainty is added to the  $t\bar{t}$  sample. The theoretical cross section uncertainty for the  $Z$  + jets and  $W$  + jets backgrounds are estimated to be  $\pm 6\%$  each with an additional 30% uncertainty on these samples due to the uncertainty on the jet to lepton fake rate. An 8% uncertainty is applied to the  $Z\gamma$  background due to the reweighting. This uncertainty is based on the statistical uncertainty of the fake ratio and estimated jet contamination of the background. The luminosity uncertainty is assigned to be 6.1%.

An uncertainty in the shape of the  $Z - p_T$  reweighting distributions is calculated by shifting the reweighting function by  $\pm 1\sigma$ . The electron  $p_T$  resolution is estimated by applying the  $\pm 1\sigma$  variation in the electron smearing function. Similarly, the muon  $p_T$  resolution is estimated by applying the  $\pm 1\sigma$  variation in the muon smearing function.

## VII. RESULTS AND SUMMARY

We see that the BDT output distributions in data agree within uncertainties with the expected backgrounds, as shown in Figure 6. The BDT output distributions for each mass point are therefore used to set limits on the Higgs boson inclusive production cross section,  $\sigma(p\bar{p} \rightarrow H + X)$ , assuming SM values for the branching ratios and for the relative cross sections of the various Higgs production mechanisms considered. We calculate the limits using a modified frequentist method (CLs), with a log-likelihood ratio (LLR) test statistic [10]. Both channels are combined in the limit, but to achieve maximal sensitivity, the two individual inputs are treated separately by the limit setting software. To minimize the degrading effects of systematics on the search sensitivity, the individual background contributions are fitted to the data observation by maximizing a profile likelihood function for the background-only and signal-plus-background hypotheses [11].

Table II presents expected and observed upper limits at 95% CL for  $\sigma(p\bar{p} \rightarrow H + X)$  relative to that expected in the SM for each Higgs boson mass considered. Figure 7 shows the expected and observed limits for  $\sigma(p\bar{p} \rightarrow H + X)$  relative to the SM for the different Higgs boson masses, while Figure 8 shows the corresponding LLR distribution.

## VIII. CONCLUSION

A search for the standard model (SM) Higgs boson was presented using a trilepton sample in  $p\bar{p}$  collisions at a center-of-mass energy of  $\sqrt{s} = 1.96$  TeV with data collected from April 2002 to September 2011 by the RunII DØ detector corresponding to  $9.7 \text{ fb}^{-1}$  of integrated luminosity. No significant excess is observed above the SM background and limits are extracted on the SM Higgs boson production cross section for a Higgs mass range of  $m_H = 100 - 200$  GeV, in intervals of 5 GeV.

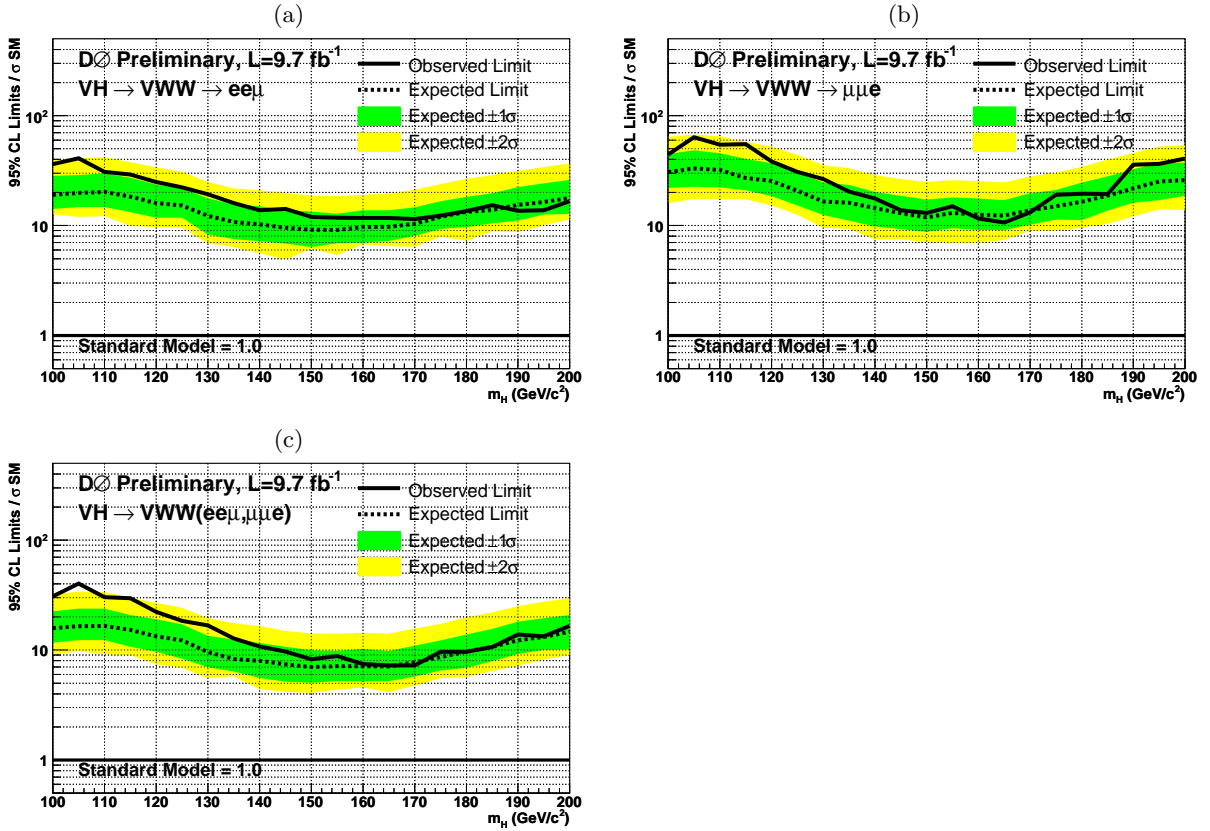


FIG. 7: Excluded cross section  $\sigma(p\bar{p} \rightarrow H + X)$  at 95% CL in units of the SM cross section as a function of  $m_H$  using (a)  $ee\mu$  channel, (b)  $\mu\mu e$  channel, and (c) combined channels.

### Acknowledgments

We thank the staffs at Fermilab and collaborating institutions, and acknowledge support from the DOE and NSF (USA); CEA and CNRS/IN2P3 (France); MON, Rosatom and RFBR (Russia); CNPq, FAPERJ, FAPESP and FUNDUNESP (Brazil); DAE and DST (India); Colciencias (Colombia); CONACyT (Mexico); NRF (Korea); FOM (The Netherlands); STFC and the Royal Society (United Kingdom); MSM and GACR (Czech Republic); BMBF and DFG (Germany); SFI (Ireland); The Swedish Research Council (Sweden); and CAS and CNSF (China).

- 
- [1] V.M. Abazov *et al.* [DØ Collaboration], Nucl. Instr. and Methods A **565**, 463 (2006).
  - [2] R. Angstadt, *et al.*, Nucl. Instr. and Methods A **622**, 298 (2010).
  - [3] S. Abachi *et al.* [DØ Collaboration], Nucl. Instrum. and Methods A **338**, 185 (1994).
  - [4] V.M. Abazov *et al.*, Nucl. Instrum. and Methods A **552**, 372-398 (2005).
  - [5] T. Sjöstrand *et al.*, Comput. Phys. Commun. **135**, 238 (2001);  
we use version 6.323 or later.
  - [6] M.L. Mangano *et al.*, JHEP **0307**, 001 (2003);  
we use version 2.11.
  - [7] R. Brun and F. Carminati, CERN Library Long Writeup, W5013, (1994).
  - [8] C. Lester and D. Summers, Phys. Lett. B **463**, 99-103 (1999).
  - [9] H. Cheng and Z. Han, JHEP **12**, 063 (2008).
  - [10] T. Junk, Nucl. Instrum. and Methods A **434**, 435 (1999).  
A. Read, CERN 2000-005 (30 May 2000).
  - [11] W. Fisher, FERMILAB-TM-2386-E.

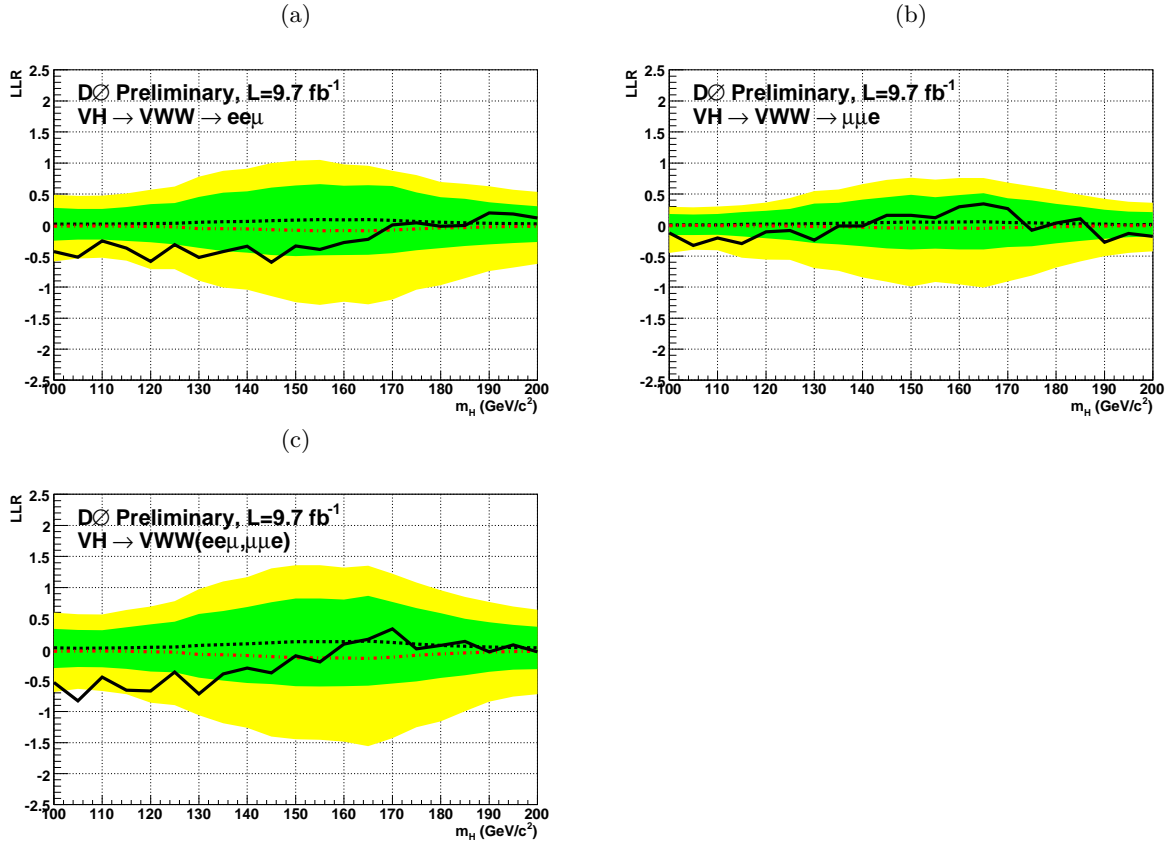


FIG. 8: The observed LLR (solid line) as a function of  $m_H$  using (a)  $ee\mu$  channel, (b)  $\mu\mu e$  channel, and (c) combined channels. Also shown are the expected LLRs for the  $B$  (black dashed line) and  $S + B$  (red dashed line) hypotheses, with the green and yellow bands indicating one and two sigma fluctuations of the expected LLR for the  $B$ -only hypothesis.